

# A G1-like globular cluster in NGC 1023 <sup>1</sup>

Søren S. Larsen

*UC Observatories / Lick Observatory, University of California, Santa Cruz, CA 95064, USA*

soeren@ucolick.org

## ABSTRACT

The structure of a very bright ( $M_V = -10.9$ ) globular cluster in NGC 1023 is analyzed on two sets of images taken with the Hubble Space Telescope. From careful modeling of King profile fits to the cluster image, a core radius of  $r_c = 0.55 \pm 0.1$  pc, effective radius  $R_e = 3.7 \pm 0.3$  pc and a central surface brightness of  $\mu_0(V) = 12.9 \pm 0.5$  mag arcsec<sup>-2</sup> are derived. This makes the cluster much more compact than  $\omega$  Cen, but very similar to the brightest globular cluster in M31, G1 = Mayall II. The cluster in NGC 1023 appears to be very highly flattened with an ellipticity of  $\epsilon \approx 0.37$ , even higher than for  $\omega$  Cen and G1, and similar to the most flattened clusters in the Large Magellanic Cloud.

*Subject headings:* galaxies: star clusters — galaxies: individual (NGC 1023)

## 1. Introduction

A very bright globular cluster in the nearby lenticular galaxy NGC 1023 was recently identified by Larsen, Brodie and Kissler-Patig (2001). At a distance of  $9.9 \pm 0.6$  Mpc (Ciardullo, Jacoby and Harris 1991), NGC 1023 is close enough that images taken with the *Hubble Space Telescope* (HST) will show globular clusters (GCs) as spatially extended objects, and the structure of individual clusters with sufficient S/N can be studied in considerable detail. It is of interest to compare the structural parameters (size, ellipticity etc.) of globular clusters in different galaxies because significant differences are known to exist even among GCs in the Local Group. For example, clusters in the Large Magellanic Cloud (LMC) are more flattened than those in the Milky Way (Geisler & Hodge 1980). It has also been noted that the *brightest* GCs in the Milky Way and M31 ( $\omega$  Cen and G1 = Mayall II, respectively), as well as in the Magellanic Clouds, are the most flattened in their respective host galaxies (van den Bergh 1984), and van den Bergh (1996) has suggested using the HST to test if the brightest globular clusters around other galaxies are also flattened. In the present paper the structure of the bright globular cluster in NGC 1023 is analyzed using archive HST images, and it is then compared with  $\omega$  Cen and G1.

---

<sup>1</sup>Based on observations obtained with the NASA/ESA Hubble Space Telescope, obtained at the Space Telescope Science Institute, which is operated by the Association of Universities for Research in Astronomy, Inc. under NASA contract No. NAS5-26555.

## 2. The bright cluster n1023-13

Larsen, Brodie and Kissler-Patig (2001) presented spectroscopy of 11 old globular clusters in NGC 1023, most of which were selected from WFPC2 exposures obtained as part of Program 6554 (PI: Brodie) and discussed in Larsen and Brodie (2000). However, a few additional objects were selected from ground-based images, one of which (n1023-13) turned out to be a very bright globular cluster. The 2000.0 coordinates are  $\alpha = 2:40:27.84$  and  $\delta = 39:04:40.2$ . Although this object is close to the saturation limit on the Brodie dataset and located near the edge of one of the WF chips, it is also included on a shorter WFPC2 exposure of NGC 1023, obtained for D. Richstone (HST Program ID 6587). This dataset consists of 5 integrations of 260 sec each in the F555W band and 2 integrations of 900 sec in the F814W band, short enough that the cluster is well below the saturation limit.

Fig. 1 shows a close-up of the Richstone WFPC2 image of the cluster, compared to a star of similar brightness. The cluster is clearly resolved and appears to be significantly elongated. At a distance of 9.9 Mpc, one WFPC2 pixels spans 4.8 pc, comparable to or somewhat larger than the typical half-light radius of a globular cluster (e.g. Kundu and Whitmore 2001), so special care must be taken when analyzing the light profile of clusters at this distance. Nevertheless, the S/N of n1023-13 is sufficient to allow a relatively detailed analysis of its structure and compare with other bright globular clusters like  $\omega$  Centauri in the Milky Way and G1 = Mayall II in M31.

### 2.1. Modeling of the light profile

Of the 5 available F555W exposures in the Richstone dataset, only two were used for the analysis presented here. The two selected exposures required no shifts in the  $x$  and  $y$  directions, and consequently no resampling of the Point Spread Function (PSF), before combination. Addition of the individual images, including elimination of cosmic ray hits, was done with the IMCOMBINE task in IRAF<sup>2</sup>. Inspection of the data quality files for the Brodie WFPC2 image showed that the image of n1023-13 was, in fact, not saturated, so we are in the fortunate situation of having two WFPC2 images of the same cluster, allowing for a useful consistency check of the results. The cluster is located on two different WF chips (WF2 on the Richstone and WF4 on the Brodie dataset), and at very different positions within the chips ( $(x, y) = 210, 560$  versus  $(x, y) = 740, 79$ ) in the two pointings.

The F555W images of the cluster were modeled using the `ishape` algorithm (Larsen 1999), assuming various analytical models for the intrinsic luminosity profile of the cluster and then convolving with the HST PSF, generated by the TinyTim software (Krist and Hook 1997). A convolution with the WFPC2 “diffusion kernel” was also included. The ellipticity, Full Width At

---

<sup>2</sup>IRAF is distributed by the National Optical Astronomical Observatories, which are operated by the Association of Universities for Research in Astronomy, Inc. under contract with the National Science Foundation

Half Maximum (FWHM) and orientation of the model profiles were iteratively adjusted until the best match with the observed image was obtained. As the TinyTim manual and *WFPC2 handbook* give two slightly different diffusion kernels, fits were done for both of them. Because the diffusion kernel is wavelength dependent but only given for the F555W filter in the manuals, no fits to the F814W images were attempted.

Two different types of analytical profiles were assumed: King (1962) profiles of the form

$$\mu(r) = k \left[ \frac{1}{\sqrt{1 + r^2/r_c^2}} - \frac{1}{\sqrt{1 + r_t^2/r_c^2}} \right]^2, \quad r < r_t \quad (1)$$

and “Moffat” profiles given as

$$\mu(r) = \mu_0 [1 + (r/r_c)^2]^{-\alpha}. \quad (2)$$

The King profiles are characterized by a core radius  $r_c$  and a tidal radius  $r_t$  and are known to provide excellent fits to globular cluster luminosity profiles. The Moffat profiles are similar to the profiles used by Elson, Fall, & Freeman (1987) to fit young LMC clusters, but note that the  $\alpha$  in Eq. (2) is equivalent to their  $\gamma/2$ . In the limiting case of  $\alpha = 1$ , Eq. (2) is identical to a King profile with infinite tidal radius.

The version of **ishape** used here allows the concentration parameter  $c = r_t/r_c$  of the King profiles and the exponent  $\alpha$  of the Moffat profiles to be kept at a fixed value, or to vary these parameters during the fitting process. The  $c$  parameter is the most uncertain of the fitted parameters, and the exact value returned by **ishape** was quite dependent on the initial guesses. Generally, the fitted  $c$  values were between 100 and 300. In order to ensure better stability in the fits and assess the effect of variations in  $c$ , the remaining shape parameters (ellipticity, FWHM, orientation) were thus determined for fixed  $c$  values of 100, 200 and 300. The Moffat fits, on the other hand, were quite stable and consistently returned  $\alpha$  values around  $1.20 \pm 0.05$ .

The fitting radius was set to 15 pixels or  $1''.5$ , corresponding to a radius of 72 pc for a distance of 9.9 Mpc. A number of fits were also done for a fitting radius of 25 pixels, but for this larger radius the background gradient becomes noticeable, although the results of the fits remained essentially identical to those done with the smaller radius.

Figure 2 shows the results of various fits to the Richstone image. From the left: King profiles with  $c = 10, 30, 100, 300$  and  $\infty$  and the best-fitting Moffat profile with  $\alpha = 1.20$ . The top row shows the best-fitting model images generated by convolution of the King/Moffat profiles with the TinyTim PSF and diffusion kernel, and the bottom row shows the residuals when the model images are subtracted from the observed image. The King profiles with  $c < 100$  or  $c = \infty$  are clearly unable to reproduce the observed cluster image, while the  $c = 100$  and  $c = 300$  profiles show little structure in the residuals beyond the photon noise. Formally, the best fit (lowest  $\chi^2$ ) was obtained for  $c \sim 200$ . Increased S/N could potentially help in constraining the King profile  $c$  parameter and for this purpose a number of fits were carried out on all 5 Richstone images combined. These tended to converge towards  $c \approx 150$ . It thus seems reasonable to adopt  $c = 200 \pm 100$  for the concentration

parameter. The  $\alpha = 1.2$  Moffat profile also provides a very good fit, but the King profile fits which are physically better motivated will be used for most of the discussion in this paper.

The various King and Moffat profiles are plotted in Fig. 3, scaled to the same luminosity within  $1''.5$  and computed for the actual fitted core radii. Note that Fig. 3 shows the *intrinsic* cluster profiles, not the observed ones (which are obtained by convolving the profiles in Fig. 3 with the HST PSF and diffusion kernel). Since 1 WF pixel spans  $0''.1$ , it is clear that the central parts of the profiles are unresolved and the differences in the fits rely mainly on the behaviour in the wings.

## 2.2. Shape parameters for best fitting King profiles

The best fit parameters are given in Table 1 for each of the two WFPC2 datasets. Each value in the Table is an average of 6 individual fits, for King profiles with  $c = 100, 200$  and  $300$ , and for the two different diffusion kernels. The quoted errors are simply the standard deviation of these individual measurements, which is probably a better estimate of the true uncertainty than the standard error on the mean.

The first rows in the Table give the photometry in a  $0''.5$  (5 pixels) aperture, corrected for reddening towards NGC 1023. The photometry was done with the PHOT task in DAOPHOT directly on the images, measuring the background as the mode of all pixels in an annulus starting at 20 pixels and 10 pixels wide. Calibration to standard  $V$  and  $I$  magnitudes was done following Holtzman et al. (1995) and using the Schlegel et al. (1998) extinction value of  $A_B = 0.262$  mag. The distance modulus of  $29.97 \pm 0.14$  derived by Ciardullo, Jacoby and Harris (1991) was based on Burstein and Heiles (1984) extinctions, which often tend to be somewhat lower than the Schlegel et al. (1998) values. However, for NGC 1023 the two happen to agree to within 0.01 mag in  $A_B$ .

For an extended object like n1023-13, the  $0''.5$  aperture slightly underestimates the total brightness. According to Holtzman et al. (1995), the WFPC2 PSF itself scatters about 10% of the light to radii beyond their  $0''.5$  reference aperture, while measurements of n1023-13 through an  $r = 20$  pixels aperture gave total  $V$  magnitudes brighter by about 0.2 mag compared to the  $r = 5$  pixels measurements. Thus, the  $V$  magnitudes in Table 1 are probably too faint by  $\sim 0.1$  mag, and after applying this correction the absolute magnitude becomes  $M_V = -10.9$ . Likewise, direct integration of the King profiles also yields a correction of about 0.1 mag from  $r = 0''.5$  to  $r = \infty$ .

There is excellent agreement between the photometry from the two pointings, as well as between the **ishape** profile fits. The two sets of fits give FWHM values of  $0''.027 \pm 0''.006$  and  $0''.029 \pm 0''.007$ , minor/major axis ratios of  $0.62 \pm 0.02$  and  $0.64 \pm 0.01$ , and the position angles on the sky agree to within 3 degrees. Note that the relatively large range in the  $c$  parameter does not lead to correspondingly large uncertainties on the fitted FWHM.

The FWHM and concentration parameter returned by **ishape** can be converted to more familiar quantities such as the core radius ( $r_c$ ) and half-light (effective) radius ( $R_e$ ). For a King profile

the FWHM and  $r_c$  are related as

$$\text{FWHM} = 2 \left[ \left( \sqrt{1/2} + \frac{1 - \sqrt{1/2}}{\sqrt{1 + c^2}} \right)^{-2} - 1 \right]^{1/2} r_c, \quad (3)$$

i.e.  $\text{FWHM} \approx 2r_c$  for  $c \gg 1$ . A similar simple analytical relation between the FWHM or  $r_c$  and  $R_e$  does not exist, but can be approximated by a power-law of the form

$$R_e/r_c \approx 0.547 c^{0.486} \quad (4)$$

For  $c > 4$  this approximation is good to  $\pm 2\%$ .

These relations assume that the profiles are circularly symmetric, while the FWHM values returned by **ishape** are measured along the major axis of the fitted profiles. In order to compute the core and effective radii in Table 1, an average of the major and minor axis FWHM has been used. This results in core radii of  $r_c = 0.52 \pm 0.12$  pc and  $r_c = 0.57 \pm 0.13$  pc for the two datasets, and effective radii of  $R_e = 3.47 \pm 0.33$  pc and  $R_e = 3.85 \pm 0.34$  pc, respectively, at the assumed distance of NGC 1023.

### 2.3. Ellipticity

The minor/major axis ratio returned by the fits is quite stable at around  $0.63 \pm 0.01$ , corresponding to a very large ellipticity of  $\epsilon = 0.37 \pm 0.01$ . An independent estimate can be obtained by using the ELLIPSE task in the STSDAS package to fit elliptical isophotes directly to the cluster image, although these will tend to underestimate the ellipticity because the true shape is blurred by the HST PSF. This effect will be worse closer to the center, while ellipse fits at large radii are uncertain because of low S/N. At  $r = 5$  pixels, the ELLIPSE task returns ellipticities of  $\epsilon = 0.24$  on both the Richstone F555W and F814W exposures, and 0.14 and 0.20 on the Brodie F555W and F814W exposures. Irregularities in the background due to the proximity to the edge of the image are clearly visible in the Brodie exposures and the ELLIPSE fits are probably less accurate for these data.

ELLIPSE fits were also done on the model images generated by **ishape** (Figure 2). These fits returned an ellipticity of  $\epsilon = 0.25$  at  $r = 5$  pixels, in nearly perfect agreement with the fits to the actual science images. Thus, it is clear that the blurring of the cluster image by the HST PSF leads to an underestimation of  $\epsilon$  when measured directly on the images, and the true answer probably lies closer to the  $\epsilon \sim 0.37$  value from the King profile fits.

### 2.4. Central surface brightness

Although the central parts of the King profiles are unresolved on the WFPC2 images, the central surface brightness for the cluster can still be computed, assuming that the King profile

continues all the way to the center. The central surface brightness  $\mu_0$  of a King (1962) profile and the total luminosity  $L(R)$  within a radius  $R < r_t$  are related as

$$\mu_0 = k \left[ 1 - \frac{1}{\sqrt{1+c^2}} \right]^2 \quad (5)$$

and

$$L(R) = \pi k \left[ r_c^2 \ln \left( 1 + \frac{R^2}{r_c^2} \right) + \frac{R^2}{1+c^2} - \frac{4r_c^2}{\sqrt{1+c^2}} \left( \sqrt{1 + \frac{R^2}{r_c^2}} - 1 \right) \right] \quad (6)$$

For reddening-corrected  $V = 19.19$  and  $V = 19.17$  within a radius of  $R = 0''.5$ , this results in  $\mu_0 = 12.8 \pm 0.4$  mag arcsec $^{-2}$  and  $\mu_0 = 13.0 \pm 0.4$  mag arcsec $^{-2}$  for the two fits. Again, the errors are computed as the standard deviation of the 6 values based on the individual fits. The computed  $\mu_0$  values are not very sensitive to the exact concentration parameter and most of the uncertainty comes from the core radius. Alternatively, one can also compute the central surface brightness for the Moffat profile fit. This yields  $\mu_0 = 13.6$  mag arcsec $^{-2}$ , somewhat fainter than for the King profile. However, a King profile is probably a better approximation to the true light profile of the cluster and a value around  $\mu_0 = 12.9 \pm 0.5$  mag arcsec $^{-2}$  may be a reasonable estimate of the central surface brightness and its associated error.

### 3. Comparison with G1 and $\omega$ Cen

Table 1 also lists a number of properties for two other bright globular clusters:  $\omega$  Cen, the brightest GC in the Milky Way, and G1 = Mayall II, the brightest known GC in M31 (Mayall and Eggen 1953). Pritchett & van den Bergh (1984) first noted a significant flattening of G1 and estimated an ellipticity of  $\epsilon = 0.22$ . Using HST images of G1, Rich et al. (1996) measured a core radius of  $r_c = 0''.170 \pm 0''.011$  or  $0.63 \pm 0.04$  pc for a distance modulus of 24.42 (Freedman & Madore 1990) and found a tidal radius of  $28''.2 = 105$  pc, corresponding to a concentration parameter  $c = 166$  and an effective radius of 4.1 pc. They obtained a central surface brightness of 13.5 mag arcsec $^{-2}$  in  $V$  and a slightly higher ellipticity ( $\epsilon = 0.25 \pm 0.02$ ) than the one reported by Pritchett & van den Bergh (1984). Also using HST images, Meylan et al. (2001) measured a somewhat smaller core radius of  $r_c = 0.52$  pc, but a larger tidal radius of 200 pc for G1. They quote a *half-mass* radius of  $r_h = 14$  pc, corresponding to an effective radius of 10 pc (Spitzer 1987, p. 16) if light traces mass, but their Table 3 indicates an effective radius closer to  $1''.18$  or 4.4 pc, in better agreement with Equation (4) which gives  $R_e = 0.52 \text{ pc} \times 0.547 (200/0.52)^{0.486} = 5.1$  pc. Contrary to Rich et al. (1996), Meylan et al. (2001) found a variation in ellipticity with radius, ranging from  $\epsilon = 0.1$  in the innermost and outermost parts, to  $\epsilon = 0.3$  at a radius of  $2''.1$  or 8 pc, with a mean of  $\epsilon \sim 0.2$ . All of the above studies agree on an integrated  $V$  magnitude of  $M_V = -10.9$ .

Most of the relevant parameters for  $\omega$  Cen are listed in the McMaster catalogue (Harris 1996). This cluster has  $M_V = -10.24$  and is also quite elongated with  $\epsilon = 0.19$  (Frenk & Fall 1982). It

is, however, more extended than G1 and has a core radius of 3.8 pc. The effective radius is 6.2 pc, somewhat larger than the typical 3 – 4 pc for globular clusters.

Compared to these two bright globular clusters in the Local Group, n1023-13 appears to be nearly an identical twin of G1. Both clusters are of comparable luminosity and their effective radii are quite similar to those for globular clusters of much lower luminosities. This is consistent with the lack of correlation between effective radius and cluster luminosity observed in the Milky Way (Djorgovski & Meylan 1994). Both G1 and n1023-13 have very compact cores and, as a result, very high central surface brightnesses. In fact, the highest central surface brightness for any Galactic globular cluster is  $\mu_0 = 14.15$  (NGC 1851, from the McMaster catalog) and  $\omega$  Cen itself has a much lower  $\mu_0 = 16.8$  mag arcsec $^{-2}$ .

From the core radius and central surface brightness, the central density  $\rho_0$  can be estimated from the relation

$$\rho_0 = \frac{3.44 \times 10^{10}}{P r_c} 10^{-0.4\mu_0(V)} (M/L) M_\odot \text{ pc}^{-3} \quad (7)$$

with  $P \approx 2$  and  $r_c$  in pc (Peterson & King 1975; Williams & Bahcall 1979). For G1 and n1023-13 this leads to  $\rho_0 = 2.0 \times 10^5 M_\odot \text{ pc}^{-3}$  and  $\rho_0 = (4.1 \pm 2.4) \times 10^5 M_\odot \text{ pc}^{-3}$ , respectively, assuming a M/L ratio of 1.6 (Illingworth 1976). Here we have used the average of the two estimates of  $\rho_0$  for n1023-13 listed in Table 1. From King-Michie models, Meylan et al. (2001) obtain a central density of  $\rho_0 = 4.7 \times 10^5 M_\odot \text{ pc}^{-3}$  for G1, in fair agreement with the estimate obtained from Eq. (7). Again, n1023-13 has a similar high central density to G1, while  $\omega$  Cen has a central density of only  $\sim 1400 M_\odot \text{ pc}^{-3}$ .

The metallicity of  $\omega$  Cen is given as  $[\text{Fe}/\text{H}] = -1.62$  in the McMaster catalogue. Metallicity estimates for G1 range between  $-1.19 \pm 0.25$  (Brodie and Huchra 1990) and  $-0.7$  (Rich et al. 1996), while Meylan et al. (2001) find an intermediate value of  $[\text{Fe}/\text{H}] = -0.95 \pm 0.09$ . For n1023-13, Larsen, Brodie and Kissler-Patig (2001) found  $[\text{Fe}/\text{H}] = -1.15 \pm 0.22$  from Keck spectroscopy, and a very similar value of  $[\text{Fe}/\text{H}] = -1.11$  from the  $V - I$  color. n1023-13 thus seems to be somewhat more metal-rich than  $\omega$  Cen, but of comparable metallicity to (or maybe slightly lower than) G1. It is also worth noting that – unlike most globular clusters – both  $\omega$  Cen and G1 have quite a large internal scatter in their metallicity distributions. Whether or not this is the case for n1023-13 is, however, impossible to tell from the current data.

One common property of all these bright globular clusters is their high ellipticities. The `ishape` fits indicate an ellipticity as high as  $\epsilon \approx 0.37$  for n1023-13.  $\omega$  Cen has an ellipticity of  $\epsilon = 0.19$ , while G1 appears to display a range of ellipticities as a function of radius, reaching a maximum of  $\epsilon = 0.30$  at intermediate radii. The present data do not permit an analysis of internal variations in the shape parameters (ellipticity, orientation) of n1023-13, but from the mean values it seems that the cluster may be even more flattened than  $\omega$  Cen and G1. Is an ellipticity  $\epsilon = 0.37$  unrealistically large? Although most globular clusters in the Milky Way have low ellipticities, clusters in the Large Magellanic Cloud tend to be much more elongated. One of the more striking examples is the intermediate-age ( $\sim 2$  Gyr) cluster NGC 1978 with an ellipticity of  $\epsilon = 0.30$  (Fischer, Welch,

& Mateo 1992). After correction for projection effects, Geisler & Hodge (1980) find that very few LMC clusters are likely to be spherical, most having true ellipticities in the range 0.2 – 0.4. Thus, the high ellipticity for n1023-13 might not be unreasonable, especially if the cluster is seen nearly edge-on, but it would definitely rank it as one of the most elliptical clusters known.

Which mechanism might be responsible for the high ellipticities of massive globular clusters? In a recent paper, Cen (2001) has argued that many globular clusters may initially possess significant amounts of angular momentum, which should cause flattening of their initial shapes (King 1961). Some evidence has been presented that rotation might indeed be a dominant mechanism in causing flattening of globular clusters (Davoust 1986; White & Shawl 1987) and of  $\omega$  Cen in particular (Meylan & Mayor 1986; Merritt, Meylan, & Mayor 1997). On the other hand, Fischer, Welch, & Mateo (1992) found no evidence for rotation in the highly flattened cluster NGC 1978, although they could not rule it out. However, it is not quite clear why this effect should affect the most massive clusters more strongly. Perhaps the tendency for more massive clusters to have longer relaxation times (Spitzer 1987, p. 40) can cause an initial flattening to persist for a longer period of time in these systems, or maybe the more massive clusters tend to be born with larger angular momenta. Detailed dynamical calculations and a better understanding of globular cluster formation will be required before these questions can be definitively answered.

Another mechanism which could produce elongated clusters with high angular momenta is merging of binary clusters (Sugimoto & Makino 1989). If the two clusters have different metallicities then the result might be an elongated cluster with a metallicity spread, as observed in  $\omega$  Cen and G1, although it seems unlikely that two clusters born near each other (in time and space) would exhibit such large metallicity differences. Alternatively, the merger might result from a later chance encounter between two clusters (Icke & Alcaïno 1988), but this clearly makes the mechanism less attractive as a general explanation.

Finally, Meylan et al. (2001) have discussed the possibility that G1 and  $\omega$  Cen are the remnants of nucleated dwarf galaxies. This might make the metallicity spread and elongated morphology of these two clusters more understandable, but does not appear to be a likely explanation for the high ellipticities of most LMC clusters.

### 3.1. Sources of errors

Comparison of the two independent fits gives a good estimate of the random errors involved in the fitting process. However, because the characteristic sizes involved are on the same order of magnitude as the resolution of the images, the fitted parameters are strongly dependent on correct modeling of the WFPC2 PSF. One critical component is the “diffusion kernel”, which takes into account charge diffusion between neighboring pixels in the CCDs. The diffusion kernel given in the TinyTim manual scatters less light to the surrounding pixels than the one in the *WFPC2 handbook*, and this difference also influences the fits. By comparison of the fits with the two different diffusion



kernels, it was found that the kernel given in the WFPC2 handbook generally gave smaller FWHM values by about 0.02 – 0.04 pixels or  $0''.002 - 0''.004$ . This is consistent with this kernel scattering more light into surrounding pixels, thus causing `ishape` to fit a slightly narrower intrinsic profile.

We also fitted the star shown in Fig. 1 with and without the diffusion kernel. When using the diffusion kernel, `ishape` was unable to improve the King model fits relative to comparison fits obtained by using a delta function, as expected for an unresolved stellar image. In contrast, if the diffusion kernel was omitted then `ishape` clearly recognized the star as an “extended” object with an effective radius of about 0.2 pixels, confirming that the “raw” TinyTim PSF underrepresents the size of a point source and that the diffusion kernel needs to be taken into account.

Errors in the distance to NGC 1023 are not included in the uncertainty estimates in Table 1. The  $9.9 \pm 0.6$  Mpc value from Ciardullo, Jacoby and Harris (1991) is based on the planetary nebula luminosity function, and agrees well with the 10.2 Mpc distance estimate given by Faber et al. (1997). Size parameters (FWHM,  $r_c$ ,  $R_e$  and  $r_t$ ) scale linearly with the distance, while the central surface brightness  $\mu_0$  is distance-independent. Thus, from Eq. 7, the central density is inversely proportional to the distance. Compared to the measurement errors, the uncertainty on the distance to NGC 1023 has only a minor effect on the results, even if the  $\pm 6\%$  error estimate by Ciardullo, Jacoby and Harris (1991) might be somewhat optimistic.

#### 4. Summary

Based on a detailed analysis of its spatial structure, the bright globular cluster n1023-13 is found to be very similar to the G1 cluster in M31. Both have an absolute  $V$  band magnitude of  $M_V = -10.9$ . Using the average values from Table 1, the spatial profile of n1023-13 is well fitted by a King model with core radius  $0.55 \pm 0.1$  pc, effective radius  $3.7 \pm 0.3$  pc and concentration parameter  $c \sim 200$ . The cluster appears to be very flattened with an ellipticity around  $\epsilon \approx 0.37$ , making it one of the flattest star clusters known, and providing another example of the van den Bergh (1984) observation that the brightest GCs in galaxies also tend to be the most flattened. Assuming that the King profile continues all the way to the cluster center, a very high central surface brightness of  $\mu_0(V) = 12.9 \pm 0.5$  mag arcsec $^{-2}$  is derived, implying a central density of  $(4.1 \pm 2.4) \times 10^5$  M $_{\odot}$  pc $^{-3}$ . This is comparable to G1, but two orders of magnitude higher than for  $\omega$  Centauri.

This work was supported by National Science Foundation grant number AST9900732. I thank Jean Brodie and Sidney van den Bergh for comments on the paper and enlightening discussions, and the referee for useful suggestions.

## REFERENCES

- Brodie, J. P. and Huchra, J. P. 1990, *AJ*, 362, 503
- Burstein, D. and Heiles, C. 1984, *ApJS*, 54, 33
- Cen, R. 2001, *ApJ*, submitted (preprint astro-ph/0101197)
- Ciardullo, R., Jacoby, G. H., and Harris, W.E. 1991, *ApJ*, 383, 487
- Davoust, E. 1986, *A&A*, 166, 177
- Djorgovski, S. & Meylan, G. 1994, *AJ*, 108, 1292
- Elson, R. A. W., Fall, S. M., and Freeman, K. C., 1987, *ApJ*, 323, 211
- Faber, S. M. et al. 1997, *AJ*, 114, 1771
- Fischer, P., Welch, D. L., & Mateo, M. 1992, *AJ*, 104, 1086
- Freedman, W. L. & Madore, B. F. 1990, *ApJ*, 365, 186
- Frenk, C. S. & Fall, S. M. 1982, *MNRAS*, 199, 565
- Geisler, D. & Hodge, P. 1980, *ApJ*, 242, 66
- Harris, W. E. 1996, *AJ*, 112, 1487
- Holtzman, J. A., Burrows, C. J., Casertano, S., et al. 1995, *PASP*, 107, 1065
- Icke, V. & Alcaïno, G. 1988, *A&A*, 204, 115
- Illingworth, G. 1976, *ApJ*, 204, 73
- King, I. R. 1961, *AJ*, 66, 68
- King, I. R. 1962, *AJ*, 67, 471
- Krist, J., and Hook, R. 1997, “The Tiny Tim User’s Guide”, STScI
- Kundu, A. and Whitmore, B. C. 2001, *AJ*, 121, 2950
- Larsen, S. S. 1999, *A&A Suppl.*, 139, 393
- Larsen, S. S., and Brodie, J. P., 2000, *AJ*, 120, 2938
- Larsen, S. S., Brodie, J. P., and Kissler-Patig, M. 2001, *AJ*, in preparation
- Lee, M. G., and Geisler, D. 1993, *AJ*, 106, 493
- Mayall, N. U., and Eggen, O. J., 1953, *PASP*, 65, 24

- Merritt, D., Meylan, G., & Mayor, M. 1997, AJ, 114, 1074
- Meylan, G. & Mayor, M. 1986, A&A, 166, 122
- Meylan, G., Sarajedini, A., Jablonka, P., et al. 2001, AJ, Aug 2001, in press (astro-ph/0105013)
- Peterson, C. J. & King, I. R. 1975, AJ, 80, 427
- Pritchett, C. and van den Bergh, S. 1984, PASP, 96, 804
- Rich, R. M., Mighell, K. J., Freedman, W. L., and Neill, J. D., 1996, AJ, 111, 768
- Schlegel, D. J., Finkbeiner, D. P., and Davis, M. 1998, ApJ, 500, 525
- Spitzer, L. 1987, “Dynamical Evolution of Globular Clusters”, Princeton Series in Astrophysics, Princeton University Press, editor: Jeremiah P. Ostriker
- Sugimoto, D. & Makino, J. 1989, PASJ, 41, 1117
- van den Bergh, S., 1984, PASP, 96, 329
- van den Bergh, S., 1996, The Observatory, 116, 103
- White, R. E. & Shawl, S. J. 1987, ApJ, 317, 246
- Williams, T. B. & Bahcall, N. A. 1979, ApJ, 232, 754

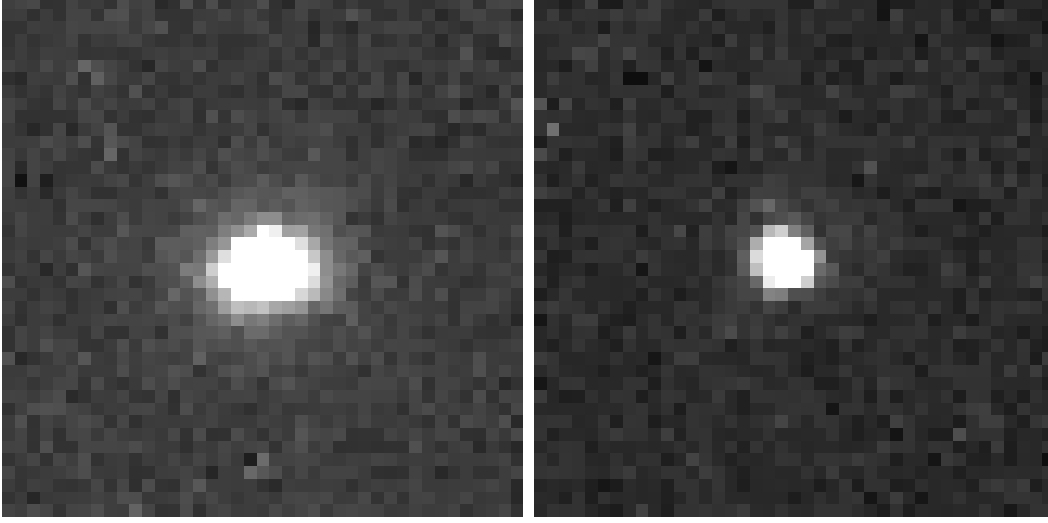


Fig. 1.— Images of the globular cluster n1023-13 (left) and a star (right). The two objects are of about the same integrated magnitude and are shown with the same contrast settings. The cluster image is clearly more extended and appears to be elongated. Each image spans  $40 \times 40$  pixels or  $4'' \times 4''$ .

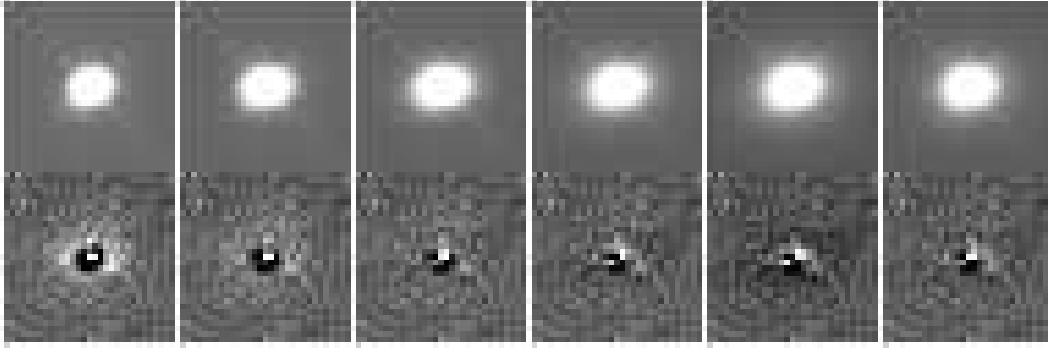


Fig. 2.— Synthetic cluster images and residuals for various analytical cluster models, fitted by *ishape*. From left to right: King ( $c = 10, 30, 100, 300, \infty$ ) and Moffat ( $\alpha = 1.20$ ).

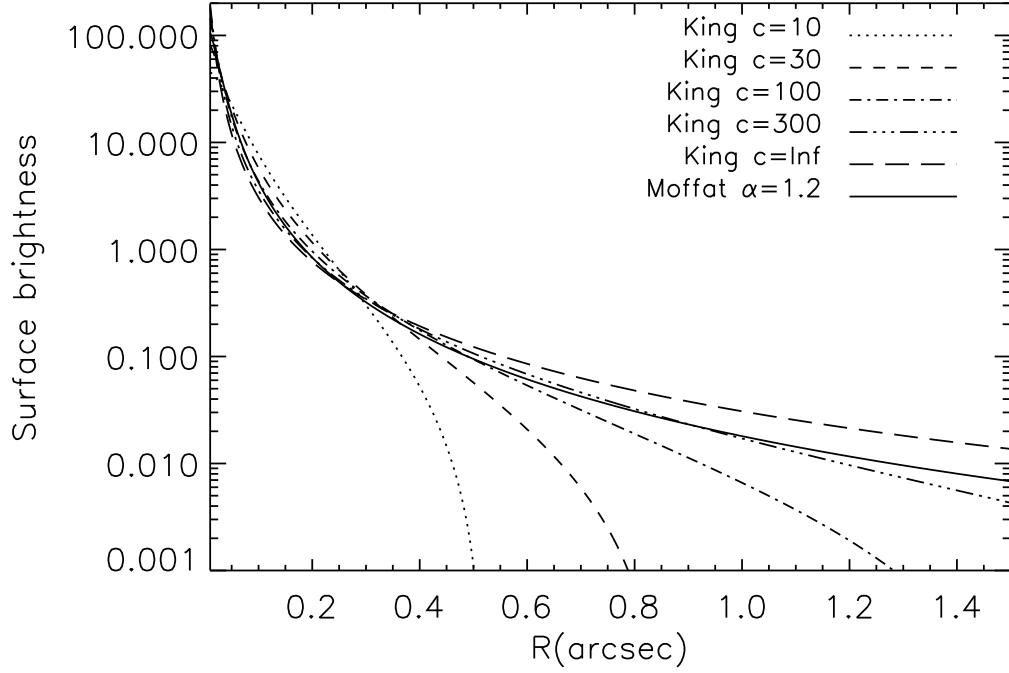


Fig. 3.— Illustration of the various luminosity profiles fitted by **ishape**. King models with concentration parameters  $c = 10, 30, 100, 300$  and  $\infty$  (dotted/dashed lines) and a MOFFAT profile with index  $\alpha = 1.20$  (solid line). All profiles have been normalized to the same luminosity within  $r = 1''.5$ . Note that these are the *intrinsic* profiles, not taking into account the fact that the actual observed profiles are blurred by the WFPC2 PSF.

Table 1. Comparison of n1023-13, G1 and  $\omega$  Cen.

	Richstone	Brodie	G1 <sup>a</sup>	$\omega$ Cen <sup>b</sup>
$V_0$	$19.190 \pm 0.005$	$19.173 \pm 0.005$	-	-
$(V - I)_0$	$1.038 \pm 0.006$	$1.050 \pm 0.006$	-	-
$M_V$	-10.9	-10.9	-10.9	-10.24
[Fe/H]	$-1.15 \pm 0.2$		-1.2...-0.7	-1.62
$c$	$200 \pm 100$		166...380	17.4
minor/major	$0.62 \pm 0.02$	$0.64 \pm 0.01$	$\sim 0.75$	0.81
P.A.	$-40.9 \text{ deg} \pm 1.1$	$-38.3 \text{ deg} \pm 1.0$	-	-
FWHM	$0''.027 \pm 0''.006$	$0''.029 \pm 0''.007$	-	-
	$1.27 \pm 0.29 \text{ pc}$	$1.39 \pm 0.32 \text{ pc}$	-	-
$r_c$ (pc)	$0.52 \pm 0.12$	$0.57 \pm 0.13$	0.52...0.63	3.8
$R_e$ (pc) <sup>c</sup>	$3.47 \pm 0.33$	$3.85 \pm 0.34$	$4.5 \pm 0.5$	6.2
$r_t$ (pc)	$95 \pm 27$	$105 \pm 30$	90...200	67
$\mu_0$ (V mag arcsec <sup>-2</sup> )	$12.8 \pm 0.4$	$13.0 \pm 0.4$	13.5	16.8
$\rho_0$ (M <sub>⊙</sub> pc <sup>-3</sup> )	$(4.7 \pm 2.8) \times 10^5$	$(3.5 \pm 2.0) \times 10^5$	$4.7 \times 10^5$	$1.4 \times 10^3$

Note. — For  $r_c$  and  $R_e$  the given values are averages of minor and major axis values.  $V_0$  and  $(V - I)_0$  are given for a  $0''.5$  (5 pixels) aperture.

$c$  = King profile concentration parameter =  $r_t/r_c$ . P.A. = Position angle on sky, measured N through E.  $\mu_0$  = central surface brightness,  $\rho_0$  = central density.

<sup>a</sup>: Tabulated values for G1 represent the range quoted in the literature. See discussion in main text for details.

<sup>b</sup>: data from the McMaster catalog (Harris 1996)

<sup>c</sup>: Computed from  $r_c$  and  $r_t$ .